Spatially Fixed and Moving Virtual Sensing Methods for Active Noise Control

Danielle J. Moreau

School of Mechanical Engineering
The University of Adelaide
South Australia 5005
Australia

A thesis submitted in fulfillment of the requirements
for the degree of Ph.D. in Mechanical Engineering
on 11 December 2009. Qualified on 12 February 2010.

Chapter 5

Virtual Energy Density Sensing in a Three-dimensional Sound Field

Minimising the acoustic energy density has a number of advantages over minimising the squared acoustic pressure in both global and local active noise control. Employing an acoustic energy density cost function has been shown to overcome the observability problems associated with reducing the squared pressure and improves the overall global attenuation achieved by minimising a potential energy density cost function estimated by microphones (Sommerfeldt and Nashif, 1994, Sommerfeldt and Parkins, 1994, Elliott and Garcia-Bonito, 1995). Minimising the acoustic energy density has also been shown to increase the size of the localised zone of quiet beyond that generated in pressure control. Elliott and Garcia-Bonito (1995) investigated the local control of both pressure and pressure gradient in a pure tone diffuse sound field with two secondary sources. Minimising both the pressure and pressure gradient along a single axis with two secondary sources produced a far-field zone of quiet over a distance of $\lambda/2$, in the direction of pressure gradient measurement. This is considerably larger than the zone of quiet obtained by minimising the pressure alone with a single secondary source (in which the 10 dB zone of quiet is limited to $\lambda/10$).

In an effort to extend the localised zone of quiet generated at a virtual location, one-dimensional virtual acoustic energy density sensors have been developed using the forward difference prediction technique (Kestell et al., 2000a) and the SOTDF virtual sensing method, as presented in Chapter 3. These one-dimensional virtual acoustic energy density sensors estimate the sound pressure and the pressure gradient along one of the three orthogonal axes. Forward difference prediction virtual

energy density sensors were shown to produce a broader region of control compared to virtual microphones in numerical simulations and experiments conducted in a free field and a long narrow duct (Kestell, 2000, Kestell et al., 2000a, Kestell et al., 2001a, Kestell et al., 2001b). Active noise control at a stochastically optimal virtual energy density sensor with two secondary sources in a pure tone diffuse sound field, generates a zone of quiet with a diameter of approximately $\lambda/2$ at the virtual location, as shown in Chapter 3. This is a five fold increase in the size of the zone of quiet compared to that obtained by cancelling the pressure at a virtual location alone.

In this chapter, a fixed three-dimensional virtual acoustic energy density sensing method is presented for use in a modally dense three-dimensional sound field. This virtual energy density sensing method uses a modified version of the remote microphone technique (Roure and Albarrazin, 1999) to create a spatially extended zone of quiet at a fixed virtual location. Experimental results of active noise control at a virtual energy density sensor and a virtual microphone are presented to compare the size of the localised zone of quiet achieved by minimising either the acoustic energy density or the squared pressure. To create a zone of quiet at the virtual energy density sensor, the remote energy density sensing technique is combined with a modified version of the filtered-x LMS algorithm for acoustic energy density sensing and is used to calculate the control signals that drive four secondary sources during real-time control. Four secondary sources are required in local acoustic energy density control to independently drive the pressure and the pressure gradients along the three orthogonal axes to zero. If only a single secondary source is used per energy density sensor there will be a trade off between the attenuation achieved at the error sensor location and the size of the localised zone of quiet.

The performance of one-dimensional virtual acoustic energy density sensors in local active noise control has been previously investigated in a free field, a long narrow duct (Kestell, 2000, Kestell et al., 2000a, Kestell et al., 2001a, Kestell et al., 2001b) and in a pure tone diffuse sound field (using the SOTDF virtual sensing method presented in Chapter 3). In many real would applications, however, it is likely that the sound field is neither perfectly free field nor perfectly diffuse. In this chapter, the performance of three-dimensional virtual acoustic energy density sensors is experimentally investigated in a modally dense three-dimensional sound field. The experimental results presented here therefore demonstrate the performance of virtual acoustic energy density sensors in a sound field that is more likely to be encountered in practice.

The secondary purpose of this study is to determine whether fixed virtual energy density sensors provide an alternative to moving virtual microphones. The moving virtual microphones developed in Chapter 4 create a moving zone of quiet that tracks an observer's ears during head rotations. As a seated observer moves their head through a relatively small region of the sound field, the spatially extended zone of quiet generated at a virtual acoustic energy density sensor may be large enough to encompass the path of the observer's ear. Minimising the acoustic energy density at a fixed virtual location may therefore be an alternative to active noise control at a moving virtual microphone.

Section 5.1 presents a derivation of the remote energy density sensing technique. The experimental method is detailed in Section 5.2, including a discussion of the modified filtered-x LMS algorithm for energy density sensing. Finally, the results of real-time experiments generating a zone of quiet at a virtual energy density sensor and a virtual microphone in a modally dense three-dimensional sound field are discussed in Section 5.3.

5.1 Theoretical background

The remote energy density technique uses a modified version of the remote microphone technique (Roure and Albarrazin, 1999) to generate a virtual energy density sensor at a spatially fixed virtual location. The total instantaneous acoustic energy density at a virtual location is given by

$$E_{D,v}(n) = \frac{1}{2}\rho\sum_{m=1}^{3} v_{v,m}^2(n) + \frac{p_v^2(n)}{2\rho c^2}, \tag{5.1}$$

where $m = 1, 2, 3$ corresponds to the x, y and z direction respectively, $v_{v,m}(n)$ is the total particle velocity at the virtual location in the mth direction, $p_v(n)$ is the total sound pressure at the virtual location, ρ is the ambient fluid density and c is the speed of sound. The remote energy density technique estimates the acoustic sound pressure, $\tilde{p}_v(n)$, and the three components of particle velocity, $\tilde{v}_{v,1}(n)$, $\tilde{v}_{v,2}(n)$, and $\tilde{v}_{v,3}(n)$, at the virtual location. The total acoustic energy density at the virtual location is then calculated using Eq. (5.1). In the following description of the remote energy density technique, estimation of the sound pressure, $\tilde{p}_v(n)$, and the general mth component of particle velocity, $\tilde{v}_{v,m}(n)$, at the virtual location is derived for simplicity. In practice, all three components of particle velocity, $\tilde{v}_{v,1}(n)$, $\tilde{v}_{v,2}(n)$, and

$\tilde{v}_{v,3}(n)$, must be calculated to obtain an estimate of the three-dimensional acoustic energy density.

The remote energy density technique calculates the acoustic pressure, $\tilde{p}_v(n)$, and the mth component of particle velocity, $\tilde{v}_{v,m}(n)$, at the virtual location using the acoustic pressure, $p_a(n)$, and the mth component of particle velocity, $v_{a,m}(n)$, measured at a physical energy density sensor. The remote energy density technique requires a preliminary identification stage in which a second acoustic energy density sensor is temporarily located at the virtual location. During the preliminary identification stage, the secondary transfer functions between the L secondary sources and each of the physical and virtual quantities, $p_a(n)$, $v_{a,m}(n)$, $p_v(n)$ and $v_{v,m}(n)$, are measured as vectors $\tilde{\mathbf{Z}}_{sa,p}$, $\tilde{\mathbf{Z}}_{sa,vm}$, $\tilde{\mathbf{Z}}_{sv,p}$ and $\tilde{\mathbf{Z}}_{sv,vm}$. The primary transfer functions between the corresponding quantities at the physical and virtual locations, $\tilde{M}_p$ and $\tilde{M}_{v,m}$, are also estimated during this preliminary identification stage. The vectors of the secondary physical transfer functions, $\tilde{\mathbf{Z}}_{sa,p}$ and $\tilde{\mathbf{Z}}_{sa,vm}$, each of length L, are given by

$$\tilde{\mathbf{Z}}_{sa,p} = \left[\begin{array}{cccc} \tilde{Z}_{s1a,p} & \tilde{Z}_{s2a,p} & \ldots & \tilde{Z}_{sLa,p} \end{array} \right], \tag{5.2}$$

$$\tilde{\mathbf{Z}}_{sa,vm} = \left[\begin{array}{cccc} \tilde{Z}_{s1a,vm} & \tilde{Z}_{s2a,vm} & \ldots & \tilde{Z}_{sLa,vm} \end{array} \right], \tag{5.3}$$

where $\tilde{Z}_{sla,p}$ is the secondary transfer function between the lth secondary source and the pressure at the physical location, and $\tilde{Z}_{sla,vm}$ is the secondary transfer function between the lth secondary source and the mth component of the particle velocity at the physical location. The vectors of the secondary virtual transfer functions, $\tilde{\mathbf{Z}}_{sv,p}$ and $\tilde{\mathbf{Z}}_{sv,vm}$, each of length L, are similarly given by

$$\tilde{\mathbf{Z}}_{sv,p} = \left[\begin{array}{cccc} \tilde{Z}_{s1v,p} & \tilde{Z}_{s2v,p} & \ldots & \tilde{Z}_{sLv,p} \end{array} \right], \tag{5.4}$$

$$\tilde{\mathbf{Z}}_{sv,vm} = \left[\begin{array}{cccc} \tilde{Z}_{s1v,vm} & \tilde{Z}_{s2v,vm} & \ldots & \tilde{Z}_{sLv,vm} \end{array} \right], \tag{5.5}$$

where $\tilde{Z}_{slv,p}$ is the secondary transfer function between the lth secondary source and the pressure at the virtual location, and $\tilde{Z}_{slv,vm}$ is the secondary transfer function between the lth secondary source and the mth component of the particle velocity at the virtual location.

A block diagram of the remote energy density technique is given in Fig. 5.1. As shown in Fig. 5.1, estimates of the primary pressure and the mth component of

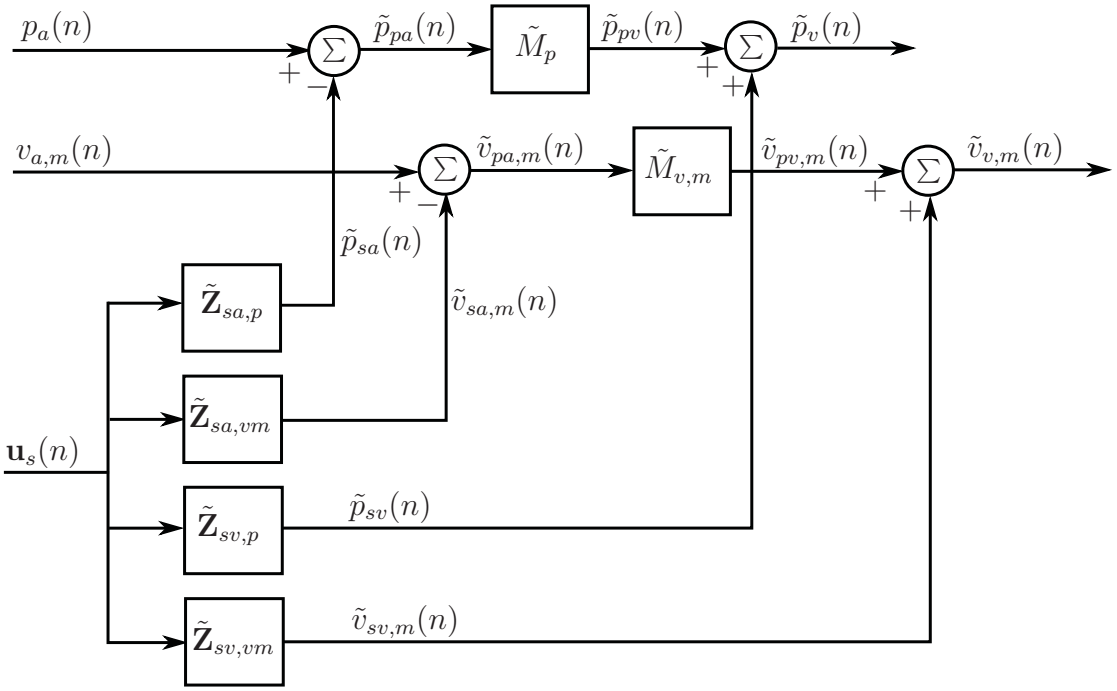

Figure 5.1: Block diagram of the remote energy density sensing technique.

the primary particle velocity, $\tilde{p}_{pa}(n)$ and $\tilde{v}_{pa,m}(n)$, at the physical location are first calculated using

$$\tilde{p}_{pa}(n) = p_a(n) - \tilde{p}_{sa}(n) = p_a(n) - \tilde{\mathbf{Z}}_{sa,p}\mathbf{u}_s(n), \tag{5.6}$$

$$\tilde{v}_{pa,m}(n) = v_{a,m}(n) - \tilde{v}_{sa,m}(n) = v_{a,m}(n) - \tilde{\mathbf{Z}}_{sa,vm}\mathbf{u}_s(n), \tag{5.7}$$

where $\tilde{p}_{sa}(n)$ is an estimate of the secondary pressure at the physical location, $\tilde{v}_{sa,m}(n)$ is an estimate of the mth component of the secondary particle velocity at the physical location and the strength of the L secondary sources is given by

$$\mathbf{u}_s(n) = \left[\begin{array}{cccc} u_{s1}(n) & u_{s2}(n) & \ldots & u_{sL}(n) \end{array} \right]^{\mathrm{T}}. \tag{5.8}$$

Next, estimates of the primary pressure and the mth component of the primary particle velocity, $\tilde{p}_{pv}(n)$ and $\tilde{v}_{pv,m}(n)$, at the virtual location are obtained using

$$\tilde{p}_{pv}(n) = \tilde{M}_p \tilde{p}_{pa}(n), \tag{5.9}$$

$$\tilde{v}_{pv,m}(n) = \tilde{M}_{v,m} \tilde{v}_{pa,m}(n). \tag{5.10}$$

Finally, estimates, $\tilde{p}_v(n)$ and $\tilde{v}_{v,m}(n)$, of the total pressure and the mth component

of the total particle velocity at the virtual location are calculated as

$$\tilde{p}_v(n) = \tilde{p}_{pv}(n) + \tilde{p}_{sv}(n) = \tilde{M}_p \tilde{p}_{pa} + \tilde{\mathbf{Z}}_{sv,p}\mathbf{u}_s(n), \tag{5.11}$$

$$\tilde{v}_{v,m}(n) = \tilde{v}_{pv,m}(n) + \tilde{v}_{sv,m}(n) = \tilde{M}_{v,m}\tilde{v}_{pa,m} + \tilde{\mathbf{Z}}_{sv,vm}\mathbf{u}_s(n), \tag{5.12}$$

where $\tilde{p}_{sv}(n)$ is an estimate of the secondary pressure at the virtual location and $\tilde{v}_{sv,m}(n)$ is an estimate of the mth component of the secondary particle velocity at the virtual location. The total acoustic energy density at the virtual location is then calculated using Eq. (5.1).

5.2 Experimental method

The performance of an active noise control system in generating a localised zone of quiet at a fixed virtual energy density sensor was investigated in real-time experiments. Active noise control was also performed at a virtual microphone to compare the size of the zone of quiet achieved by minimising the acoustic energy density and the squared pressure at a virtual location. In acoustic pressure control, the virtual microphone was generated using the remote microphone technique (Roure and Albarrazin, 1999) as presented in Section 2.1.3.

Experiments were conducted in the three-dimensional cavity shown in Fig. 4.3 with dimensions of 1000 mm × 800 mm × 890 mm. In the cavity, an electret microphone was mounted to the stepper-motor driven Cartesian traverse shown in Fig. 3.4 to enable scanning of the sound field. Details of this stepper-motor traverse have been given in Section 3.2.3. Prior to active noise control and after convergence of the controller, the sound field was scanned over three horizontal xy planes separated by a distance of 20 mm, as shown in Fig. 5.2. Each of the horizontal planes measured 120 mm in the x direction and 100 mm in the y direction and contained 143 equally spaced measurement points. The three horizontal measurement planes were located at a height of $z = 0$ mm, corresponding to the height of the sensors and at $z = \pm 20$ mm, corresponding to a height 20 mm above and below the sensors. The measurement process was repeated for active noise control being conducted at three different virtual locations within the cavity. Each of the three virtual locations were randomly selected to be at least 100 mm from the cavity walls. The experimental setup at each virtual location was such that the relative arrangement of the sensors remained constant.

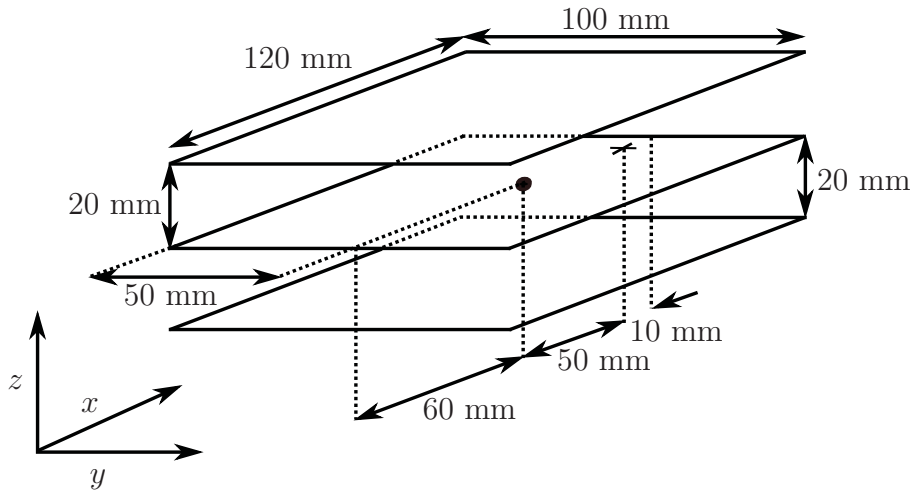

Figure 5.2: The three horizontal measurement planes. The solid round marker indicates the position of the virtual sensor while the cross indicates the position of the physical sensor. The pitch of the measurement points was 10 mm.

5.2.1 Sensor configuration

The acoustic energy density sensors used in these experiments were based on the acoustic vector sensors developed by Lockwood and Jones (2006). The energy density sensors consisted of an omnidirectional microphone (Knowles EK-3132) and three orthogonally oriented gradient microphones (Knowles NR-3158) collocated on a thin square metal rod as shown in Fig. 5.3. The energy density sensor head comprised of the four microphones occupied a volume of approximately 2 cm^3. These energy density sensors directly measure the pressure and the three orthogonal components of pressure gradient. To calculate the total instantaneous acoustic energy density in Eq. (5.1), each of the three orthogonal components of the particle velocity need to be calculated from the corresponding orthogonal components of the pressure gradient. Each of the orthogonal components of particle velocity are related to the corresponding component of pressure gradient through Euler's equation (Nelson and Elliott, 1992) by

$$v_m(n) = \frac{-1}{\rho} \int g_m(n) dn, \tag{5.13}$$

where $g_m(n)$ is the mth component of the pressure gradient. As suggested by Park and Sommerfeldt (1997), the integration required in Eq. (5.13) can be performed using a digital integrator such that the velocity estimate is calculated using the

following recursive formula

$$\tilde{v}_m(n) = \tilde{v}_m(n-1) - \frac{g_m(n)}{\rho f_s} exp\left(\frac{-1}{fs}\right), \tag{5.14}$$

where f_s is the sampling frequency.

The remote energy density sensing technique uses the error signal from a remotely located energy density sensor to obtain an estimate of the acoustic energy density at the fixed virtual location. In experiments, the physical acoustic energy density sensor was located 50 mm from the virtual location in the x direction. The remote energy density technique requires that a second acoustic energy density sensor be located at the virtual location during the preliminary identification stage. Once the preliminary identification stage is complete, the energy density sensor at the virtual location is removed. In acoustic pressure control, the physical microphone was similarly located 50 mm from the virtual location in the x direction. To obtain an estimate of the acoustic pressure at the virtual location, the remote microphone technique requires a second microphone be placed at the virtual location during the preliminary identification stage. This microphone is removed once the preliminary identification stage is complete.

The acoustic energy density sensors and the microphones were connected to a power supply and an amplifier. The amplified error signals were then sent through a 16-bit PCI-DAS1602/16 multifunction analog & digital I/O Board from Measurement Computing, which was used as a 16-channel AD-converter.

5.2.2 Actuator configuration

Five 4" loudspeakers were located in the corners of the three-dimensional cavity, one to generate the tonal primary sound field and the other four to act as the secondary sources in acoustic energy density control. The virtual acoustic energy density sensor measures the acoustic sound pressure and the three orthogonal components of the pressure gradient at the virtual location. As these are four independent quantities, four secondary sources are required to drive the acoustic energy density to zero. The loudspeakers were each excited by control signals which were first passed through a 16-bit PCI-DDA08/16 analog output board from Measurement Computing. This output board was used as an 8-channel DA-converter and an amplifier.

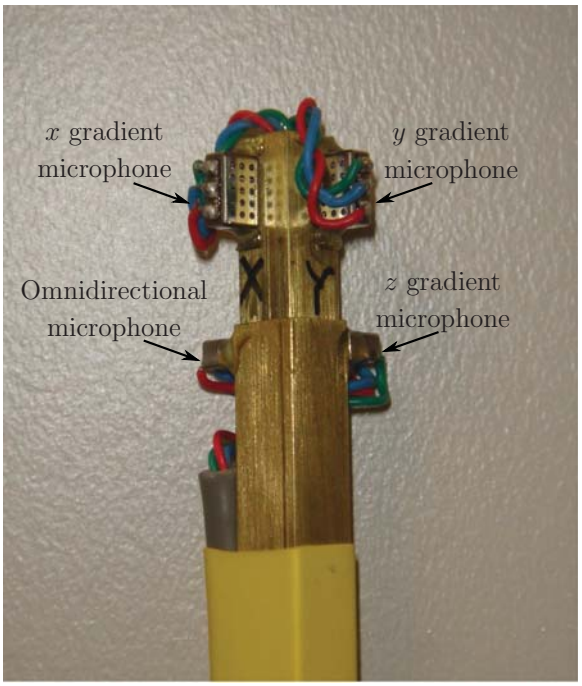

Figure 5.3: The acoustic energy density sensor consisting of an omnidirectional microphone and three orthogonally orientated pressure gradient microphones collocated on a thin metal rod.

The performance of the virtual energy density sensing algorithm was investigated at the off resonant excitation frequency of 538 Hz. At this frequency, the modal overlap is $M > 4$ illustrating that the sound field is modally dense, as a modal overlap of $M = 3$ defines the boundary between low and high modal density (Nelson and Elliott, 1992). Off resonance excitation of a modally dense sound field results in a number of residual modes contributing to the cavity response and represents the situation most commonly found in practice.

In acoustic energy density control, the control signal to drive the secondary loudspeakers, $\mathbf{u}_s(n)$, was generated using a modified version of the filtered-x LMS algorithm for energy density sensing and this algorithm is discussed as follows in Section 5.2.3. In acoustic pressure control, only one secondary source is required to minimise the acoustic pressure at the virtual location. The control signal to drive the single secondary loudspeaker, $u_s(n)$, is generated using the filtered-x LMS algorithm and this algorithm is presented in Section 5.2.4.

5.2.3 The filtered-x LMS algorithm for energy density control

Sommerfeldt and Nashif (1994) developed a modified version of the filtered-x LMS algorithm for controlling the global energy in a sound field. This control algorithm is used to generate the control signal that drives a single secondary source to minimise the measured acoustic energy density. The filtered-x LMS algorithm for energy based control is extended here for the case of minimising the estimated acoustic energy density, $\tilde{E}_{D,v}(n)$, at the virtual location with L secondary sources.

When L secondary sources are used to minimise the estimated acoustic energy density at the virtual location, the filtered-x LMS algorithm is given by

$$\mathbf{w}(n+1) = \mathbf{w}(n) - \mu \left(\sum_{m=1}^{3} \rho v_m(n) \tilde{\mathbf{r}}_{v,vm}(n) + \frac{1}{\rho c^2} \tilde{p_v}(n) \tilde{\mathbf{r}}_{v,p}(n) \right), \tag{5.15}$$

where $\mathbf{w}(n)$ is a matrix of size $LH \times 1$ of the H control filter coefficients and is defined as

$$\mathbf{w}(n) = \left[\begin{array}{cccc} \mathbf{w}_1^{\mathrm{T}}(n) & \mathbf{w}_2^{\mathrm{T}}(n) & \ldots & \mathbf{w}_L^{\mathrm{T}}(n) \end{array} \right]^{\mathrm{T}}, \tag{5.16}$$

μ is the convergence coefficient and $\tilde{\mathbf{r}}_{v,vm}(n)$ and $\tilde{\mathbf{r}}_{v,p}(n)$ are matrices of size $LH \times 1$ of the H filtered reference signals and are defined as

$$\tilde{\mathbf{r}}_{v,vm}(n) = \left[\begin{array}{cccc} \tilde{\mathbf{r}}_{v1,vm}^{\mathrm{T}}(n) & \tilde{\mathbf{r}}_{v2,vm}^{\mathrm{T}}(n) & \ldots & \tilde{\mathbf{r}}_{vL,vm}^{\mathrm{T}}(n) \end{array} \right]^{\mathrm{T}}, \tag{5.17}$$

$$\tilde{\mathbf{r}}_{v,p}(n) = \left[\begin{array}{cccc} \tilde{\mathbf{r}}_{v1,p}^{\mathrm{T}}(n) & \tilde{\mathbf{r}}_{v2,p}^{\mathrm{T}}(n) & \ldots & \tilde{\mathbf{r}}_{vL,p}^{\mathrm{T}}(n) \end{array} \right]^{\mathrm{T}}. \tag{5.18}$$

The vector of the H control filter coefficients for the lth secondary source required in Eq. (5.16), is given by

$$\mathbf{w}_l(n) = \left[\begin{array}{cccc} w_{l,0}(n) & w_{l,1}(n) & \ldots & w_{l,H-1}(n) \end{array} \right]^{\mathrm{T}}. \tag{5.19}$$

As required in Eqs. (5.17) and (5.18), vectors of the mth filtered velocity reference signals, $\tilde{\mathbf{r}}_{vl,vm}(n)$, and the filtered pressure reference signals, $\tilde{\mathbf{r}}_{vl,p}(n)$, at the virtual location are given by

$$\tilde{\mathbf{r}}_{vl,vm}(n) = \left[\begin{array}{cccc} \tilde{r}_{vl,vm}(n) & \tilde{r}_{vl,vm}(n-1) & \ldots & \tilde{r}_{vl,vm}(n-H+1) \end{array} \right]^{\mathrm{T}}, \tag{5.20}$$

$$\tilde{\mathbf{r}}_{vl,p}(n) = \left[\begin{array}{cccc} \tilde{r}_{vl,p}(n) & \tilde{r}_{vl,p}(n-1) & \ldots & \tilde{r}_{vl,p}(n-H+1) \end{array} \right]^{\mathrm{T}}. \tag{5.21}$$

Each of the m filtered velocity reference signals, $\tilde{r}_{vl,vm}(n)$, are obtained by filtering a reference signal which is strongly correlated with the primary disturbance, $x(n)$, by the transfer function, $\tilde{Z}_{slv,vm}$, between the lth secondary source and the mth component of particle velocity at the virtual location. Similarly, the filtered pressure reference signal, $\tilde{r}_{vl,p}(n)$, is obtained by filtering the reference signal, $x(n)$, by the lth virtual secondary pressure transfer function $\tilde{Z}_{slv,p}$.

The control signal to the secondary sources is now calculated as

$$\mathbf{u}_s(n) = \mathbf{X}^{\mathrm{T}}(n)\mathbf{w}(n), \tag{5.22}$$

with the matrix of reference signals $\mathbf{X}(n)$, of size $LH \times L$, being given by

$$\mathbf{X}(n) = \begin{bmatrix} \mathbf{x}(n) & 0 & \dots & 0 \\ 0 & \mathbf{x}(n) & \dots & 0 \\ \vdots & & \ddots & \\ 0 & 0 & \dots & \mathbf{x}(n) \end{bmatrix}, \tag{5.23}$$

where the vector of the H reference signals, $\mathbf{x}(n)$, is defined as

$$\mathbf{x}(n) = \begin{bmatrix} x(n) & x(n-1) & \dots & x(n-H+1) \end{bmatrix}^{\mathrm{T}}. \tag{5.24}$$

5.2.4 The filtered-x LMS algorithm for acoustic pressure control

In acoustic pressure control, the filtered-x LMS algorithm is used to generate the control signal, $u_s(n)$, that drives the secondary source to minimise the estimated virtual error signal, $\tilde{p}_v(n)$. This adaptive algorithm requires a reference signal, $x(n)$, that is highly correlated with the primary disturbance and uses the virtual error signal, $\tilde{p}_v(n)$, as feedback.

The filtered-x LMS algorithm is given by (Nelson and Elliott, 1992)

$$\mathbf{w}(n+1) = \mathbf{w}(n) - \mu\tilde{\mathbf{r}}_v(n)\tilde{p}_v(n), \tag{5.25}$$

where $\mathbf{w}(n)$ is the vector of the H controller filter coefficients given by

$$\mathbf{w}(n) = \begin{bmatrix} w_0(n) & w_1(n) & \dots & w_{H-1}(n) \end{bmatrix}^{\mathrm{T}}, \tag{5.26}$$

μ is the convergence coefficient and $\tilde{\mathbf{r}}_v(n)$ is a vector of H filtered reference signals given by

$$\tilde{\mathbf{r}}_v(n) = \begin{bmatrix} \tilde{r}_v(n) & \tilde{r}_v(n-1) & \dots & \tilde{r}_v(n-H+1) \end{bmatrix}^{\mathrm{T}}, \tag{5.27}$$

where $\tilde{r}_v(n)$ is the virtual filtered reference signal. The virtual filtered reference signal, $\tilde{r}_v(n)$, is obtained by filtering a reference signal which is strongly correlated with the primary disturbance, $x(n)$, by the virtual secondary transfer function between the virtual microphone and the secondary source.

The control signal to the secondary source is now calculated as

$$u_s(n) = \mathbf{x}^{\mathrm{T}}(n)\mathbf{w}(n), \tag{5.28}$$

where the vector of H reference signals $\mathbf{x}(n)$ is defined as

$$\mathbf{x}(n) = \begin{bmatrix} x(n) & x(n-1) & \dots & x(n-H+1) \end{bmatrix}^{\mathrm{T}}. \tag{5.29}$$

5.2.5 Real-time implementation

In both acoustic energy density and pressure control, the virtual sensing algorithms and the filtered-x LMS algorithms were implemented in real-time using xPC Target (Mathworks, 2007a,b). Details of the xPC Target system have been previously given in Section 4.2.4.

5.3 Results

Contour plots of the attenuation achieved in acoustic energy density control and acoustic pressure control at the three different virtual locations are shown in Figs. 5.4 - 5.9. In these figures, contours have been plotted at increments of 1 dB and labelled every 10 dB. Additionally, the 10 dB zone of quiet is indicated with a black dotted line. The attenuation achieved with the two control schemes over the horizontal plane at $z = 20$ mm, corresponding to a height 20 mm above the sensors, is shown in Part (a) of Figs. 5.4 - 5.9. Part (b) of Figs. 5.4 - 5.9 shows the attenuation achieved in acoustic energy density and pressure control over the horizontal plane at $z = 0$ mm, corresponding to the height of the sensors. In these figures, the virtual sensor location is indicated by the solid round marker while the cross indicates the position of the physical sensor. Part (c) of Figs. 5.4 - 5.9 shows the attenuation achieved with the two control schemes over the horizontal plane at $z = -20$ mm,

corresponding to a height 20 mm directly below the sensors.

Fig. 5.4 shows the control performance in the sound field when the acoustic energy density is minimised at the first virtual location with four secondary sources. In the $z = 0$ plane, the location of maximum attenuation is centred on the virtual location with 24 dB of attenuation being achieved at this position, as shown in Fig. 5.4 (b). The 10 dB zone of quiet is approximately oval in shape with a diameter of 60 mm in the x direction and a diameter of 40 mm in the y direction. In the $z = 20$ mm plane, the 10 dB zone of quiet is reduced to a size of approximately 30 mm in x direction and 35 mm in the y direction and the maximum attenuation achieved is 20 dB, as shown in Fig. 5.4 (a). Due to the modal distribution of the sound field, the 10 dB zone of quiet and the location of maximum attenuation have been shifted approximately 10 mm in the x and y directions from the x and y positions of the virtual location (the virtual location has a position of $x = 0$, $y = 0$, $z = 0$ in Figs. 5.4 - 5.9). In the horizontal plane 20 mm below the plane of the sensors, the 10 dB zone of quiet extends approximately 30 mm in both the x and y directions, as shown in Fig. 5.4 (c). Again the 10 dB zone of quiet and the location of maximum attenuation have been shifted from the x and y positions of the virtual location to be a distance of 10 mm away in the x direction and 20 mm away in the y direction. The maximum level of attenuation generated in the $z = -20$ mm plane is 15 dB.

The attenuation generated in the sound field with acoustic pressure control at the first virtual location is shown in Fig. 5.5. Comparing Figs. 5.4 and 5.5 shows that increased control performance is achieved in the sound field when the acoustic energy density is minimised at the virtual location with four secondary sources compared to minimising the virtual pressure with a single secondary source. In the $z = 0$ plane, virtual pressure control generates a maximum attenuation of 21 dB at the virtual location and a 10 dB zone of quiet that extends approximately 60 mm in the x direction and 20 mm in the y direction, as shown in Fig. 5.5 (b). Compared to virtual acoustic energy density control, this is a 4 dB reduction in the maximum attenuation achieved at the virtual location. The 10 dB zone of quiet has also been reduced by 20 mm in the y direction. In the $z = 20$ mm plane, virtual acoustic pressure control generates a 10 dB zone of quiet that extends approximately 15 mm in the x direction and 9 mm in the y direction, as shown in Fig. 5.5 (a). The maximum attenuation level measured in the $z = 20$ mm plane is 10 dB. In comparison to the control performance achieved in the $z = 20$ mm plane with virtual acoustic energy density control, the maximum level of attenuation is reduced by 10 dB with virtual pressure control. The 10 dB zone of quiet is also reduced in size by 15 mm in the x direction

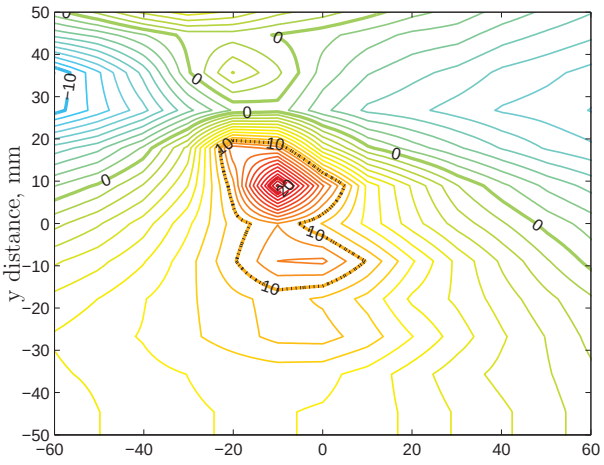

(a) $z = 20$ mm

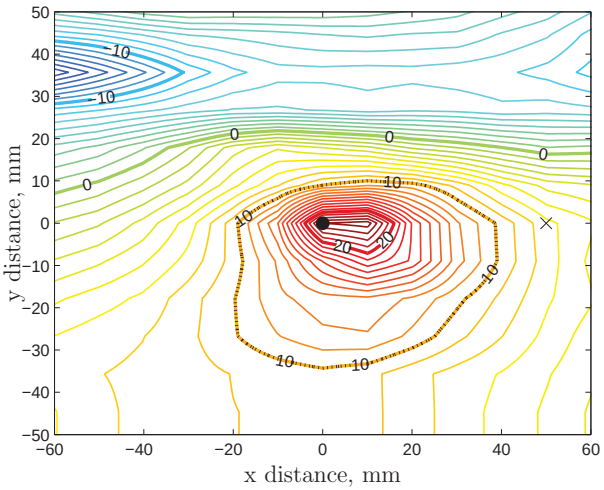

(b) $z = 0$ mm

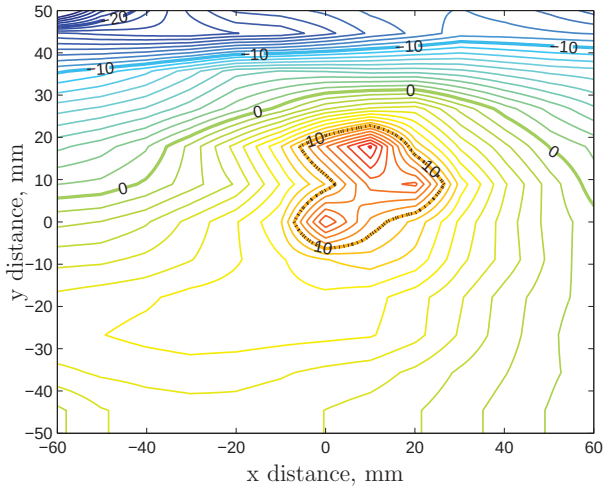

(c) $z = -20$ mm

Figure 5.4: Contour plot of the attenuation in dB achieved in acoustic energy density control at the first virtual location with four secondary sources. The virtual energy density sensor location is indicated by the solid round marker while the cross indicates the position of the physical energy density sensor.

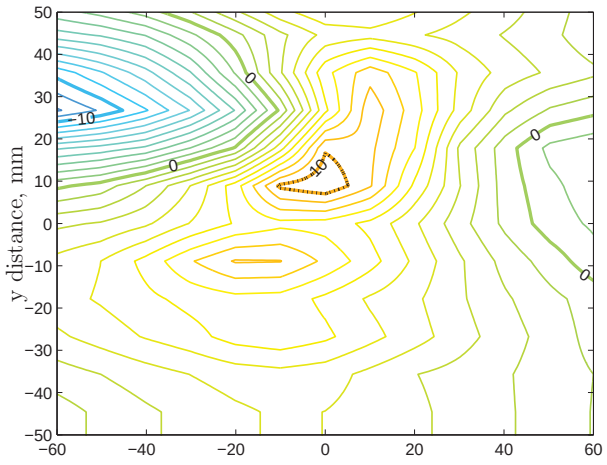

(a) $z = 20$ mm

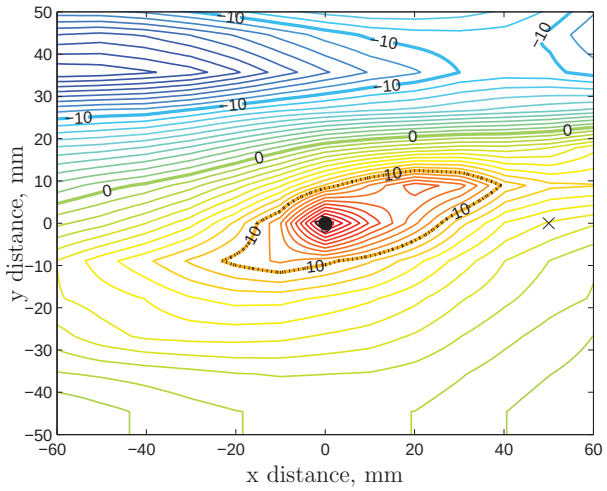

(b) $z = 0$ mm

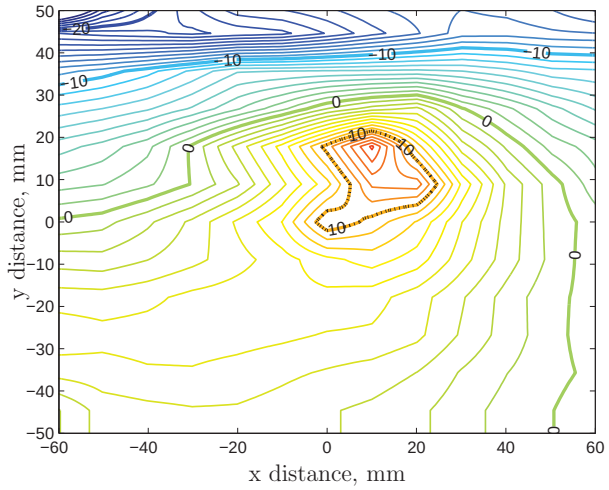

(c) $z = -20$ mm

Figure 5.5: Contour plot of the attenuation in dB achieved in acoustic pressure control at the first virtual location with a single secondary source. The virtual microphone location is indicated by the solid round marker while the cross indicates the position of the physical microphone.

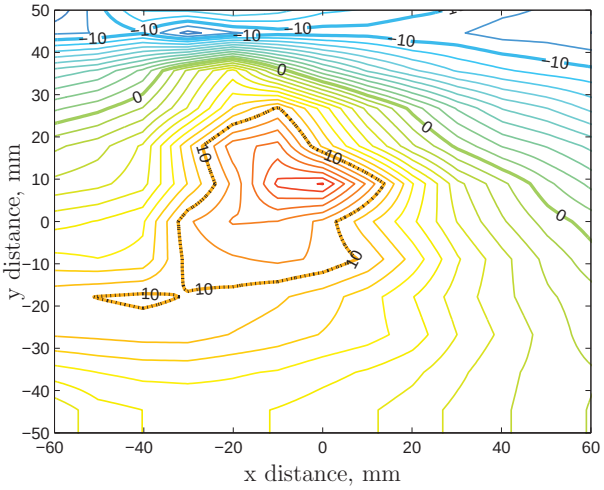

(a) $z = 20$ mm

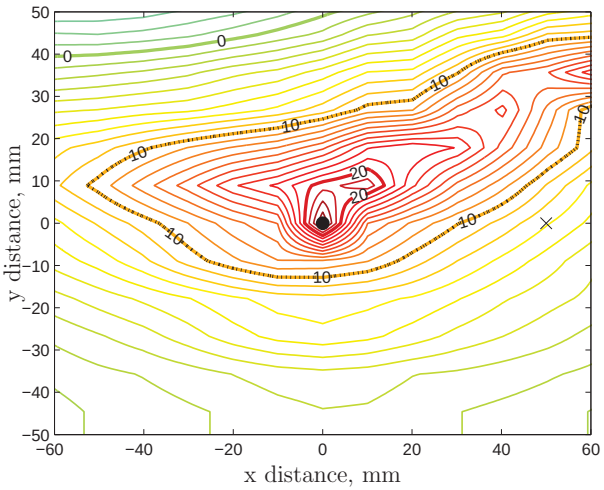

(b) $z = 0$ mm

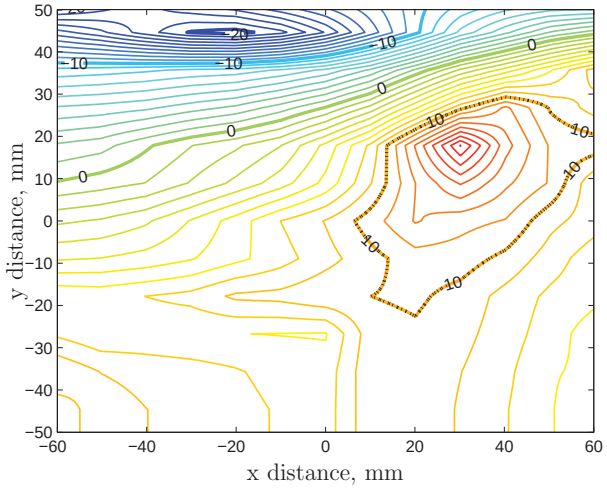

(c) $z = -20$ mm

Figure 5.6: Contour plot of the attenuation in dB achieved in acoustic energy density control at the second virtual location with four secondary sources. The virtual energy density sensor location is indicated by the solid round marker while the cross indicates the position of the physical energy density sensor.

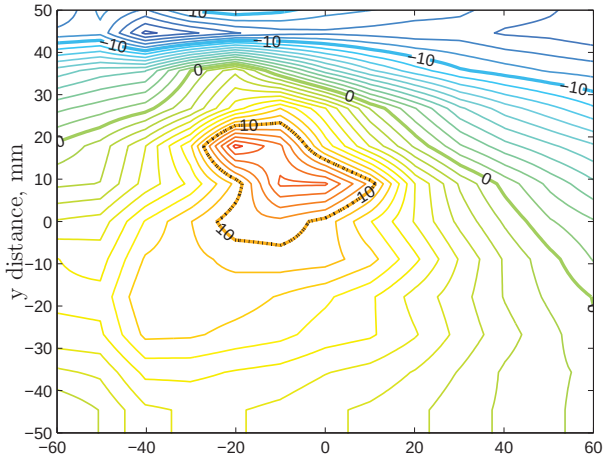

(a) $z = 20$ mm

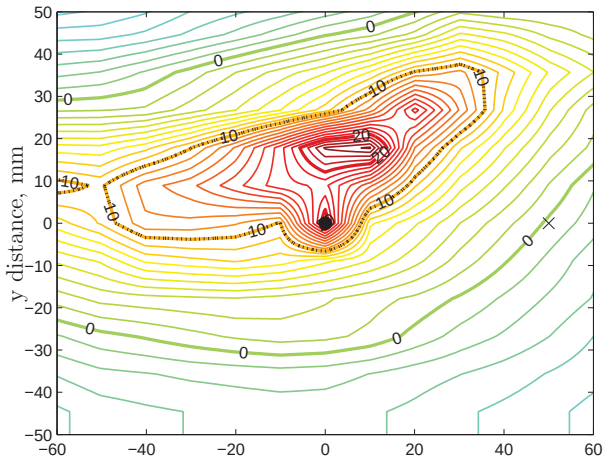

(b) $z = 0$ mm

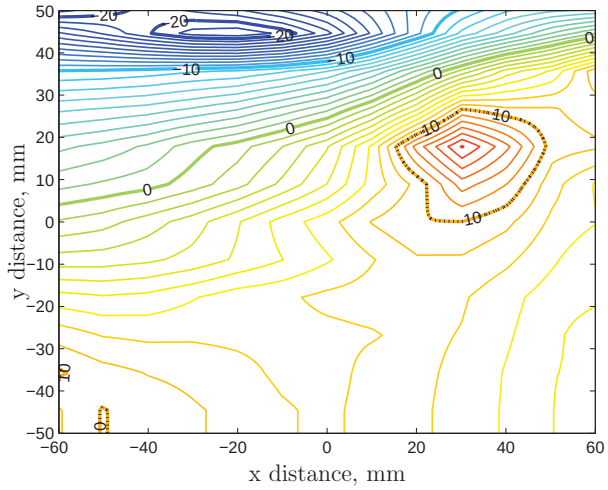

(c) $z = -20$ mm

Figure 5.7: Contour plot of the attenuation in dB achieved in acoustic pressure control at the second virtual location with a single secondary source. The virtual microphone location is indicated by the solid round marker while the cross indicates the position of the physical microphone.

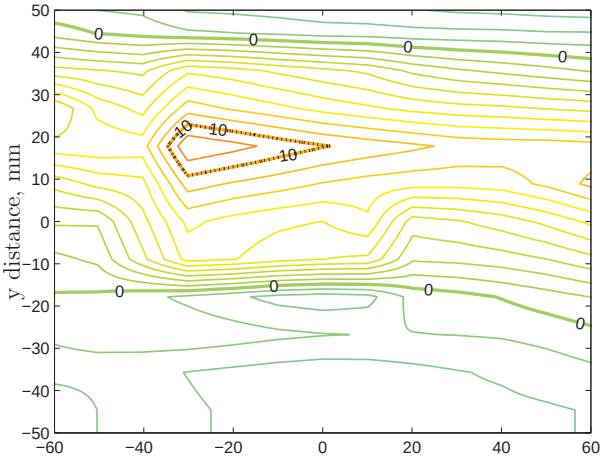

(a) $z = 20$ mm

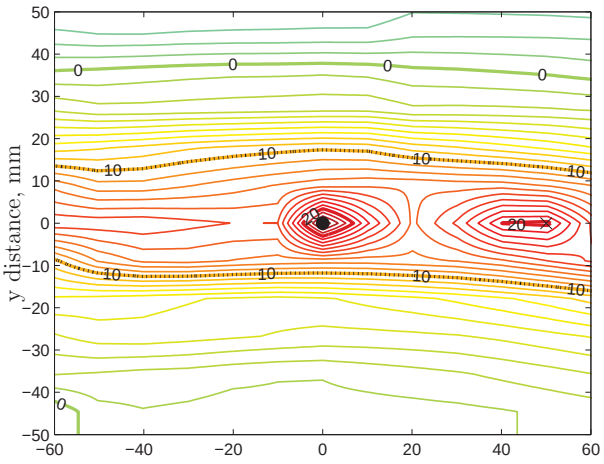

(b) $z = 0$ mm

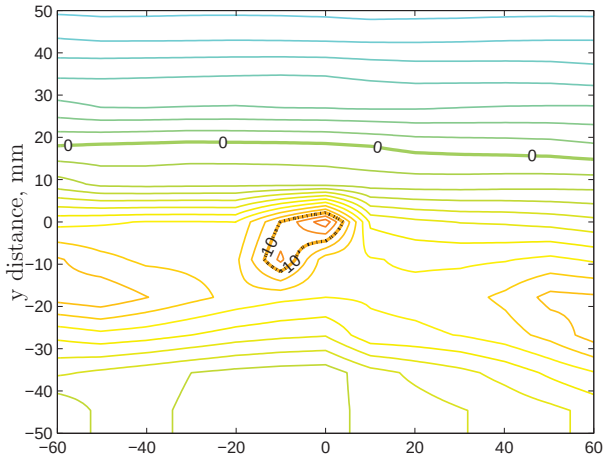

(c) $z = -20$ mm

Figure 5.8: Contour plot of the attenuation in dB achieved in acoustic energy density control at the third virtual location with four secondary sources. The virtual energy density sensor location is indicated by the solid round marker while the cross indicates the position of the physical energy density sensor.

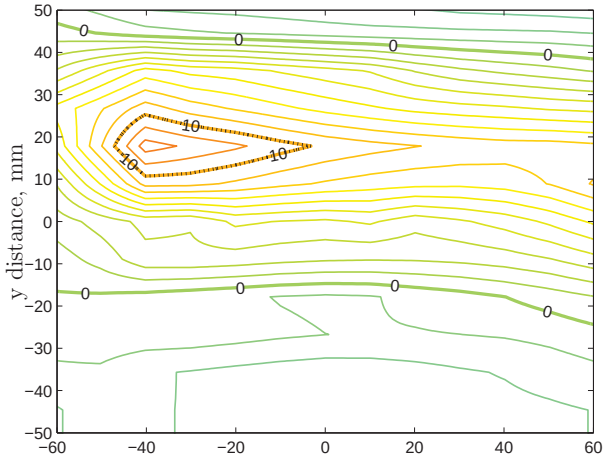

(a) $z = 20$ mm

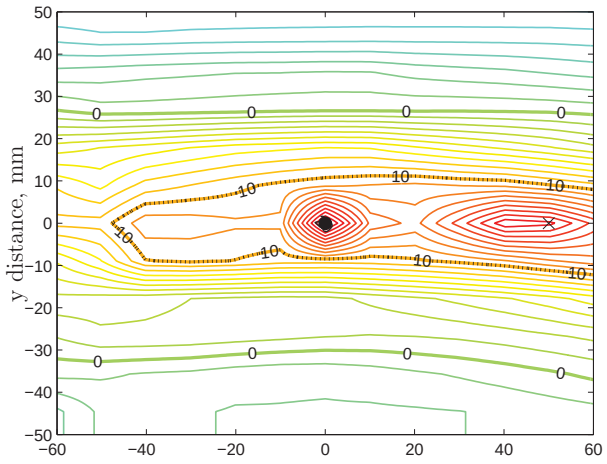

(b) $z = 0$ mm

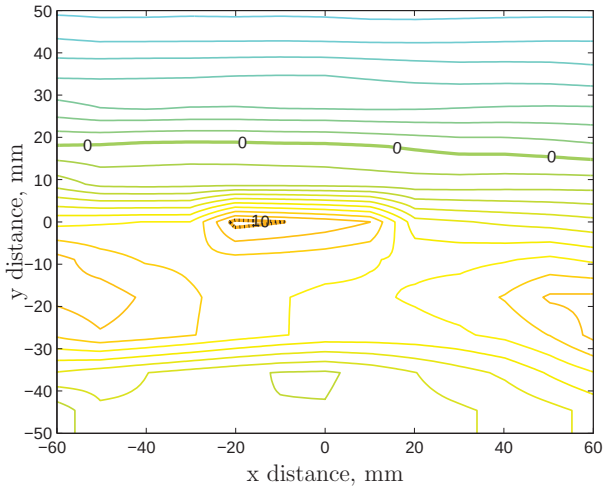

(c) $z = -20$ mm

Figure 5.9: Contour plot of the attenuation in dB achieved in acoustic pressure control at the third virtual location with a single secondary source. The virtual microphone location is indicated by the solid round marker while the cross indicates the position of the physical microphone.

and 26 mm in the y direction. In the $z = -20$ mm plane, minimising the acoustic pressure at the virtual location generates a maximum attenuation level of 15 dB and a 10 dB zone of quiet that extends 23 mm in both the x and y directions, as shown in Fig. 5.5 (c). While the maximum level of attenuation is the same in this plane for both control strategies, acoustic energy density control generates a 10 dB zone of quiet that extends 7 mm further in both the x and y directions. As seen in acoustic energy density control, the 10 dB zone of quiet generated in acoustic pressure control has been shifted slightly in the x and y directions from the x and y positions of the virtual location in both the $z = 20$ mm and the $z = -20$ mm planes.

The attenuation generated in the sound field when the acoustic energy density is minimised at the second virtual location with four secondary sources is shown in Fig. 5.6. Comparing Figs. 5.4 and 5.6 shows that the attenuation generated in the sound field with acoustic energy density control at the second virtual location is significantly greater than that achieved with active noise control at the first virtual location. This indicates that the position of the sensors within the sound field has an affect on the control performance of the active noise control system. In the $z = 0$ plane, the maximum level of attenuation generated in acoustic energy density control is 23 dB and this occurs at the virtual location, as shown in Fig. 5.6 (b). The 10 dB zone of quiet is asymmetrical and is approximately 115 mm at its widest part in the x direction and 40 mm at its widest part in the y direction. In the $z = 20$mm plane, the 10 dB zone of quiet is centred on the x and y positions of the virtual location and is reduced to a size of approximately 42 mm in x direction and 41 mm in the y direction, as shown in Fig. 5.6 (a). The maximum attenuation achieved at this height is 16 dB and this occurs at a distance of 10 mm in the y direction from the y position of the virtual location. In the horizontal plane 20 mm below the plane of the sensors, the 10 dB zone of quiet extends approximately 50 mm in both the x and y directions, as shown in Fig. 5.6 (c). Again, the 10 dB zone of quiet has been shifted from the x and y positions of the virtual location to be a distance of 30 mm away in the x direction and 20 mm away in the y direction. The maximum level of attenuation generated in the $z = -20$ mm plane is 18 dB.

Fig. 5.7 shows the control performance achieved in the sound field with acoustic pressure control at the second virtual location. Comparing Figs. 5.6 and 5.7 again shows that a greater level of attenuation is achieved in the sound field when acoustic energy density control is implemented with four secondary sources instead of acoustic pressure control with a single secondary source. In the $z = 0$ plane, virtual pressure

control generates a maximum attenuation of 20 dB at the virtual location and an asymmetrical 10 dB zone of quiet that extends approximately 78 mm at its widest part in the x direction and 35 mm at its widest part in the y direction, as shown in Fig. 5.7 (b). Compared to virtual acoustic energy density control, this is a 3 dB reduction in the maximum attenuation achieved at the virtual location. The 10 dB zone of quiet has also been reduced by 37 mm in the x direction and 5 mm in the y direction. In the $z = 20$ mm plane, virtual acoustic pressure control generates a 10 dB zone of quiet that extends approximately 30 mm in the x direction and 25 mm in the y direction, as shown in Fig. 5.7 (a). The maximum attenuation level measured in the $z = 20$ mm plane is 16 dB. In comparison to the control performance generated in the $z = 20$ mm plane with acoustic energy density control, the same level of maximum attenuation is achieved in acoustic pressure control, however the 10 dB zone of quiet is reduced in size by 12 mm in the x direction and 16 mm in the y direction. In the $z = -20$ mm plane, minimising the acoustic pressure at the virtual location generates a maximum attenuation level of 16 dB and a 10 dB zone of quiet that extends 30 mm in the x direction and 25 mm in the y direction, as shown in Fig. 5.7 (c). In this plane, the maximum level of attenuation is increased by 2 dB with acoustic energy density control, and the 10 dB zone of quiet extends a further 20 mm in the x direction and 25 mm in the y direction. As seen in acoustic energy density control, the 10 dB zone of quiet generated in acoustic pressure control has been shifted 30 mm in the x direction and 20 mm in the y direction from the x and y positions of the virtual location in the $z = -20$ mm plane due to the modal distribution of the sound field.

The attenuation achieved in the sound field when the acoustic energy density is minimised at the third virtual location with four secondary sources is shown in Fig. 5.8. In the $z = 0$ plane, the maximum attenuation level is 25 dB and occurs at the virtual location, as shown in Fig. 5.8 (b). Due to the modal distribution of the sound field around the third virtual location, significant levels of attenuation are also achieved at the physical sensor location. The 10 dB zone of quiet is centred on the virtual location and extends beyond the horizontal measurement plane in the x direction and is 38 mm wide in the y direction. In the plane 20 mm above the sensors, the 10 dB zone of quiet is reduced to a size of approximately 40 mm in x direction and 15 mm in the y direction, as shown in Fig. 5.8 (a). Due to the modal distribution of the sound field, the 10 dB zone of quiet and the location of maximum attenuation have been shifted approximately 20 mm in the x and y directions from the x and y positions of the virtual location. At this height, the

maximum attenuation achieved is 11 dB. In the horizontal plane 20 mm below the sensors, the 10 dB zone of quiet extends approximately 20 mm in the x direction and 15 mm in the y direction, as shown in Fig. 5.8 (c). The 10 dB zone of quiet and the location of maximum attenuation are centered on the x and y positions of the virtual location with the maximum level of attenuation being 12 dB.

Fig. 5.9 shows the control performance in the sound field with virtual acoustic pressure control at the third virtual location in the cavity. Comparing Figs. 5.8 and 5.9 again shows that a greater level of attenuation is achieved in the sound field when the acoustic energy density is minimised at the virtual location instead of the acoustic pressure. In the $z = 0$ plane, virtual pressure control generates a maximum attenuation of 20 dB at the virtual location and a 10 dB zone of quiet that extends beyond the horizontal measurement plane in the x direction and is 20 mm wide in the y direction, as shown in Fig. 5.9 (b). Compared to virtual acoustic energy density control, this is a 5 dB reduction in the maximum attenuation achieved at the virtual location. The 10 dB zone of quiet has also been reduced by 18 mm in the y direction. In the $z = 20$ mm plane, virtual acoustic pressure control generates a 10 dB zone of quiet that extends approximately 40 mm in the x direction and 15 mm in the y direction and the maximum attenuation level is 12 dB, as shown in Fig. 5.9 (a). This is the same sized 10 dB zone of quiet generated in acoustic energy density control and a 1 dB increase in the maximum attenuation level. As seen in acoustic energy density control, the 10 dB zone of quiet and the location of maximum attenuation generated in acoustic pressure control have both been shifted slightly in the x and y directions from the x and y positions of the virtual location in the $z = 20$ mm plane. In the horizontal plane 20 mm below the sensors, minimising the acoustic pressure at the virtual location generates a maximum attenuation level of 10 dB and a 10 dB zone of quiet that extends 12 mm in the x direction and 2 mm in the y direction, as shown in Fig. 5.9 (c). In comparison, acoustic energy density control generates a 10 dB zone of quiet that extends a further 8 mm in the x direction and 13 mm in the y direction.

5.4 Conclusion

In this chapter, a fixed virtual acoustic energy density sensing method has been presented for use in a three-dimensional sound field. The virtual energy density sensing algorithm developed in this chapter creates a spatially extended zone of quiet at a fixed virtual location using a modified version of the remote microphone

technique.

The size of the zone of quiet achieved by minimising either the acoustic energy density or the squared pressure at a virtual location has been experimentally investigated in a modally dense three-dimensional sound field. In real-time experiments, active noise control with the remote energy density sensing technique and four secondary sources was compared to active noise control with the remote microphone technique and a single secondary source. Experimental results of active noise control at three different virtual locations demonstrated that minimising the virtual acoustic energy density provides improved attenuation in the sound field and a larger 10 dB zone of quiet at the virtual location than virtual microphones.

While the zone of quiet generated at the fixed virtual energy density sensor is noticeably larger than that generated at a virtual microphone, it is still very small, with its size dependent on the source and sensor location within the sound field. Only when the moving virtual location is restricted to a very small region within the sound field would a fixed virtual energy density sensor be a comparable alternative to a moving virtual microphone.

A possible extension to this study could be the development of a moving virtual acoustic energy density sensor. Although active noise control at a moving virtual acoustic energy density sensor would not provide any significant increase to the level of attenuation achieved at the virtual location with a moving virtual microphone, it would allow for much slower tracking of the adaptive feedforward control algorithm, since the spatial variance of an acoustic energy density cost function is significantly less than that of squared pressure (Sommerfeldt et al., 1995), the control filter coefficients do not need to be updated as quickly as required in acoustic pressure control.

On a final note, it is also worth considering whether there is any advantage to using a three-dimensional acoustic energy density sensor to four closely spaced microphones arranged to span the three Cartesian axes in active noise control. The experimental results in Chapter 3 obtained with the SOTDF virtual sensing technique in a diffuse sound field indicate that minimising the one-dimensional acoustic energy density at a point or the pressures at two closely spaced locations with two secondary sources results in the same sized zone of quiet at the sensor locations. The advantage in minimising the acoustic energy density lies with observability problems that may arise when measuring the acoustic pressure at discrete locations. Placing the pressure microphones near the pressure nodes of a mode means that the mode cannot be sensed by the active noise control system and that it may be excited to

high amplitudes during control. This does not occur, however, when sensing the acoustic energy density as the velocity amplitude is large at a pressure node and therefore the mode can be sensed by the active noise control system (Sommerfeldt and Nashif, 1994).

Chapter 6

Conclusions and Future Research

6.1 Conclusions

The general aim of the research presented in this thesis is to improve and extend the spatially fixed and moving virtual sensing algorithms developed for active noise control thus far and hence increase the scope and application of local active noise control systems. In local active noise control, virtual sensors move the localised zone of quiet from the physical error sensor to a desired location. The motivation for the development of virtual sensors stems from the problems associated with local active noise control, namely that the zone of quiet generated at the error sensor is impractically small requiring the error sensor be placed at the desired location of attenuation, which is often inconvenient.

To achieve the research aim, a number of novel spatially fixed and moving virtual sensing algorithms have been presented in this thesis for active noise control. Firstly, the Stochastically Optimal Tonal Diffuse Field (SOTDF) virtual sensing method was derived. With this virtual sensing method, stochastically optimal virtual microphones and virtual energy density sensors were developed for the most complex sound field to control: a diffuse sound field. Secondly, a number of moving virtual sensing algorithms were presented. These algorithms create a zone of quiet that can track a moving virtual location in a three-dimensional sound field. The third major contribution of this thesis is development of the remote energy density technique. This virtual sensing algorithm creates a spatially extended zone of quiet at a desired location in a three-dimensional sound field using local energy density as the cost function. The main conclusions arising from these three contributions are discussed as follows.

6.1.1 The Stochastically Optimal Tonal Diffuse Field (SOTDF) virtual sensing method

The first major contribution of this thesis is development of the SOTDF virtual sensing method for a pure tone diffuse sound field. With this virtual sensing method, a stochastically optimal estimate of the pressure or the acoustic energy density is obtained at the virtual location using the error signals from a number of remotely located physical microphones or acoustic energy density sensors. This virtual sensing method is a fixed gain technique that only requires measurement of the relative distances between the sensors.

Analytical models for the controlled sound fields generated with a number of conventional control strategies and those employing the SOTDF virtual sensors were also derived. These expressions were validated using numerical simulations and experimental measurements from a reverberation chamber. Results of numerically simulated and post-processed experimental control demonstrated that increasing the number of secondary sources and the number of quantities to be minimised generates larger zones of quiet at the physical or virtual locations. This size increase will, however, most likely be accompanied by an increase in the sound pressure level away from the point of cancellation with control.

SOTDF virtual sensors were shown to accurately estimate the pressure and pressure gradient at a virtual location and to effectively shift the zone of quiet away from the physical sensors to the virtual location. In numerically simulated and post-processed experimental control, both virtual microphones and virtual energy density sensors achieved higher attenuation at the virtual location than conventional control strategies employing their physical counterpart. Minimising the pressures at four points or the pressure and pressure gradient at two points with four secondary sources was shown to achieve similar levels of attenuation at the virtual location to a virtual energy density sensor and outperform a virtual microphone. With control, the pressure level away from the point of cancellation will, however, most likely be significantly higher when four secondary sources are used.

In post-processed experimental control, the performance of control strategies employing multiple sensors and secondary sources was adversely affected by ill-conditioning. Two methods of improving the conditioning were investigated. Firstly, poorly conditioned data sets were removed from the calculation of the average zone of quiet, and secondly, one more control source than necessary was added to the control system which added another constraint to the cost function; controller effort. Both

methods significantly improved the experimental control performance so that results of post-processed experimental control agreed with the analytical and numerically simulated results.

6.1.2 Moving virtual microphone methods in a three-dimensional sound field

In this thesis, three moving virtual sensing algorithms were developed: the remote moving microphone technique; the adaptive LMS moving virtual microphone technique; and the SOTDF moving virtual sensing method. These algorithms create a zone of quiet that tracks a three-dimensional trajectory in a three-dimensional sound field. An estimate of the sound pressure at a moving virtual location is obtained with the moving virtual sensing algorithms, using the error signals from a number of remotely located spatially fixed physical microphones. Minimising the estimated error signal at the moving virtual location with the active noise control system creates a zone of quiet at the moving virtual location.

To determine the level of attenuation that can be expected at the ear of a human observer in practice, the performance of these moving virtual sensing algorithms in creating a moving zone of quiet at a single ear of a rotating artificial head was experimentally investigated in a modally dense three-dimensional cavity. Results of real-time experiments conducted both on and off resonance demonstrated that moving virtual sensors provide improved attenuation at the moving virtual location compared to either fixed virtual sensors or fixed physical sensors. The remote moving microphone technique was shown to outperform the adaptive LMS moving virtual microphone technique and the SOTDF moving virtual sensing method in terms of the level of attenuation achieved at the ear of the rotating artificial head.

The performance of the adaptive LMS moving virtual microphone technique was investigated with four different configurations of physical microphones to determine which configuration results in the most accurate estimate of the moving virtual error signal. Arranging four physical microphones in tetrahedral formation was shown to produce the most accurate estimate of the sound pressure at the moving virtual location and to generate the greatest attenuation at the ear of the rotating artificial head during real-time control.

Both the remote moving microphone technique and the adaptive LMS moving virtual microphone technique were found to be adversely effected by changes in the sound field that alter the transfer functions between the sources and the error

sensors. Recalibration of the transfer functions or the physical sensor weights is required in these moving virtual sensing algorithms if any of the error sensor or source locations are altered.

In real-time experiments, active noise control at the SOTDF moving virtual sensors was shown to provide improved attenuation at the ear of the rotating artificial head compared to either fixed SOTDF virtual sensors or fixed physical sensors in a modally dense sound field. This demonstrates that SOTDF virtual sensors are suitable for use in a sound field that is not perfectly diffuse. While the SOTDF moving virtual sensing method was outperformed by the remote moving microphone technique and the adaptive LMS moving virtual microphone technique in terms of the control performance at the moving virtual location, it is robust to changes in the sound field that may alter the transfer functions between the error sensors and the sources. An added advantage of this moving virtual sensing method is that it is much simpler to implement being a fixed weighting technique requiring only sensor position information.

6.1.3 Virtual energy density sensing in a three-dimensional sound field

A fixed virtual acoustic energy density sensing method was developed in this thesis for use in a three-dimensional sound field. The virtual energy density sensing algorithm creates a spatially extended zone of quiet at a fixed virtual location using a modified version of the remote microphone technique (Roure and Albarrazin, 1999).

Real-time experiments were conducted in a three-dimensional cavity to compare active noise control at a virtual energy density sensor using four secondary sources with active noise control at a virtual microphone using a single secondary source. Experimental results demonstrated that minimising the virtual acoustic energy density provides improved attenuation in the sound field and a larger 10 dB zone of quiet at the virtual location than virtual microphones.

As virtual acoustic energy density control creates a spatially extended zone of quiet at the virtual location, it is possible that virtual acoustic energy density sensors may provide an alternative to moving virtual microphones. If the moving virtual location is restricted to a very small region within the sound field then the zone of quiet generated at a virtual acoustic energy density sensor may be large enough to encompass the path of the virtual location.

6.2 Future research

The research presented in this thesis has led to a number of possible further research tasks and these are discussed in the following sections.

6.2.1 Stochastically optimal broadband diffuse sound field virtual sensing

In this thesis, the SOTDF virtual sensing method was developed for use in a pure tone diffuse sound field. A possible extension to this work is derivation of prediction algorithms for stochastically optimal virtual microphones and energy density sensors in a broadband diffuse sound field. Rafaely (2001) has theoretically analysed the spatial extent of the localised zones of quiet generated at a physical microphone in a broadband diffuse sound field. Using a previously derived expression for the correlation coefficient applicable to both broadband and pure tone diffuse sound fields (Rafaely, 2000), expressions for the zone of quiet generated in both the near-field and far-field of the secondary source were derived. Using the broadband diffuse field theory derived by Rafaely (2001), prediction algorithms for stochastically optimal virtual microphones and energy density sensors could be derived for broadband diffuse sound fields.

6.2.2 Effect of a headform on the size of the diffuse field zone of quiet

Garica-Bonito and Elliott (1995b) theoretically investigated the performance of the virtual microphone arrangement in cancelling the pressure at a virtual location near the surface of a reflecting sphere in a diffuse sound field. It was shown that the presence of the reflecting sphere increases the size of the zone of quiet when using the virtual microphone arrangement, especially at high frequencies. This is due to the imposed zero pressure gradient on the reflecting surfaces. The impact of generating a zone of quiet at a SOTDF virtual sensor located near the surface of a reflecting sphere in a diffuse sound field is yet to be investigated. It is expected that the performance of stochastically optimal virtual sensors would be improved by the presence of the sphere in terms of the size of the zone of quiet created at the virtual location.

6.2.3 Moving virtual sensing in a three-dimensional sound field

In this thesis, the remote moving microphone technique, the adaptive LMS moving virtual microphone technique and the SOTDF moving virtual sensing method have been developed to create a zone of quiet capable of tracking a three-dimensional trajectory in a three-dimensional sound field. The performance of these moving virtual sensing algorithms in generating a moving zone of quiet has been experimentally investigated in a modally dense three-dimensional cavity both on and off resonance. The ability of these algorithms to generate a zone of quiet at a moving virtual location in a broadband sound field is yet to be analysed or experimentally investigated. Also moving virtual sensing algorithms that employ acoustic energy density sensors are yet be developed for either tonal or broadband sound fields.

6.2.4 Moving zones of quiet at an observer's two ears

In this thesis, the performance of three moving virtual sensing methods in generating a moving zone of quiet at the single ear of a rotating artificial head has been experimentally investigated. In practice, the sound field would need to be attenuated at both ears of a human observer. Therefore, the performance of these moving virtual sensing algorithms in a generating a moving zone of quiet at each of the ears of the rotating artificial head needs to be investigated.

6.2.5 Physical sensor configurations for the adaptive LMS moving virtual microphone technique

The performance of the adaptive LMS moving virtual microphone technique was investigated with four different configurations of physical sensors including three physical microphones in linear formation perpendicular and parallel to the head motion, three physical microphones in triangular configuration and four physical microphones in tetrahedral formation. The question now arises, are there other configurations of physical sensors which would produce a more accurate estimate of the error signal at the moving virtual location. Also of consideration is whether physical sensor configurations containing more than four microphones actually improve the estimate of the moving virtual error signal. Four microphones should be sufficient to adequately model the three-dimensional sound field as only four variables are required to describe it; the sound pressure and the three orthogonal components of

particle velocity. Therefore, using more than four physical microphones may not increase the accuracy of the pressure estimate and may instead cause the conditioning of the estimation problem to become worse.